Accepted Manuscript

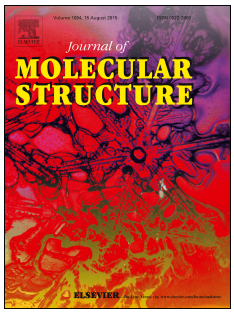

Syntheses, crystal structures, antibacterial activities of Cu(II) and Ni(II) complexes based on terpyridine polycarboxylic acid ligand

Xiaoting Wang, Ruiying Li, Aogang Liu, Caipeng Yue, Shimin Wang, Jiajia Cheng, Jinpeng Li, Zhongyi Liu

PII: S0022-2860(19)30202-9

DOI: https://doi.org/10.1016/j.molstruc.2019.02.072

Reference: MOLSTR 26229

To appear in: *Journal of Molecular Structure*

Received Date: 7 January 2019

Revised Date: 17 February 2019

Accepted Date: 18 February 2019

Please cite this article as: X. Wang, R. Li, A. Liu, C. Yue, S. Wang, J. Cheng, J. Li, Z. Liu, Syntheses, crystal structures, antibacterial activities of Cu(II) and Ni(II) complexes based on terpyridine polycarboxylic acid ligand, *Journal of Molecular Structure* (2019), doi: https://doi.org/10.1016/j.molstruc.2019.02.072.

Graphical abstract: Synopsis

Syntheses, crystal structures, antibacterial activities of Cu(II) and Ni(II) complexes based on terpyridine polycarboxylic acid ligand

Xiaoting Wang,[a] Ruiying Li,[a] Aogang Liu,[a] Caipeng Yue,[b] Shimin Wang,[c] Jiajia Cheng,[a] Jinpeng Li*,[a] Zhongyi Liu[a]

Six complexes have been synthesized and characterized. **1-3** display 1-D chain structures. **4** and **5** exhibit 2-D frameworks and **6** is a mononuclear structure. The antibacterial activities of **1-6** against four strains bacteria have been examined. The relationship between the structures of complexes and antibacterial activities was studied.

* Corresponding author. E-mail: ljp-zd@zzu.edu.cn.

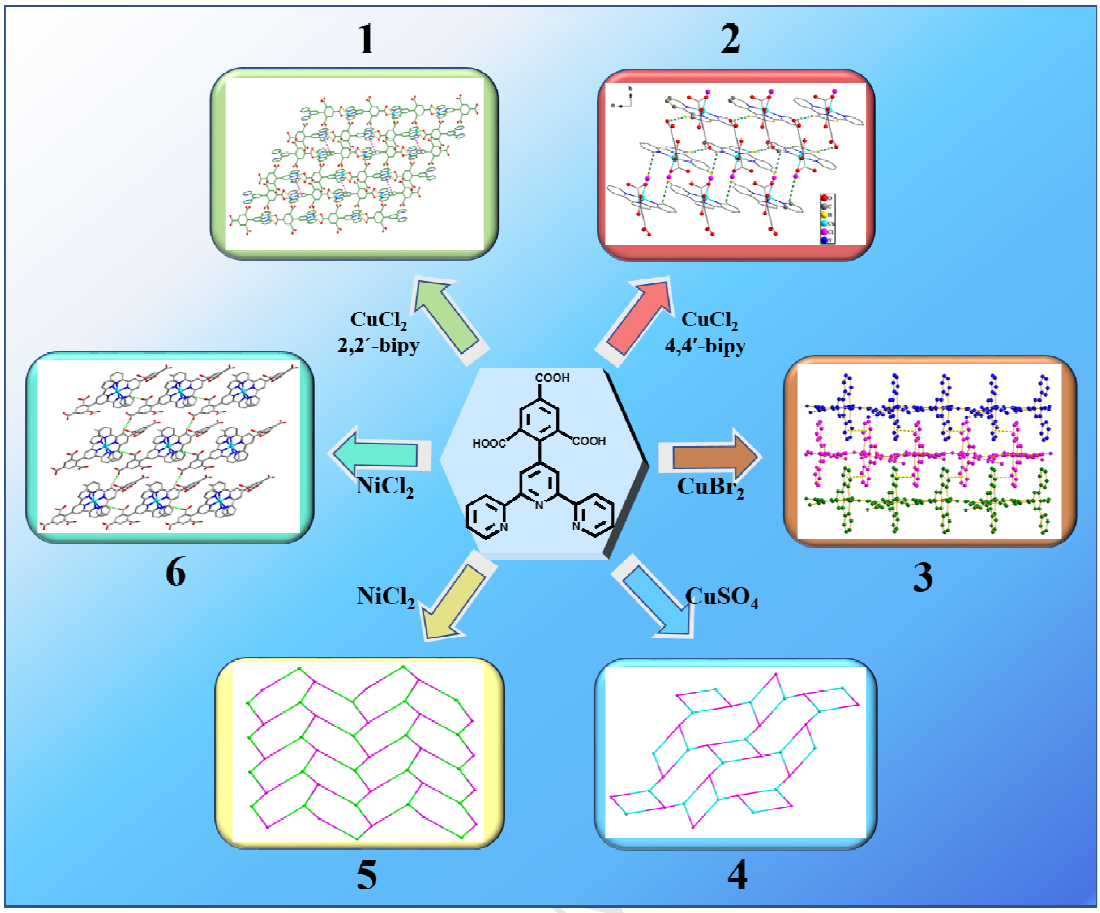

Syntheses, crystal structures, antibacterial activities of Cu(II) and Ni(II) complexes based on terpyridine polycarboxylic acid ligand

Xiaoting Wang,[a] Ruiying Li,[a] Aogang Liu,[a] Caipeng Yue,[b] Shimin Wang,[c] Jiajia Cheng,[a] Jinpeng Li[*],[a] Zhongyi Liu[a]

[a]*College of Chemistry and Molecular Engineering, Zhengzhou University, Zhengzhou 450001, Henan, P. R. China*

[b]*School of Life Sciences, Zhengzhou University, Zhengzhou, 451191, Henan, P. R. China*

[c]*College of Material and Chemistry Engineering, Henan Institute of Engineering, Zhengzhou, 451191, PR China*

Abstract

Six metal complexes $[Cu(Htpt)]_n$ (**1**), $\{[Cu(H_{1.5}tpt)Cl_{0.5}(H_2O)_{0.5}]\cdot 1/5H_2O\}_n$ (**2**), $\{[Cu(H_2tpt)(H_2O)]\cdot 1/2SO_4\cdot 2H_2O\}_n$ (**3**), $[Cu(Htpt)]_n$ (**4**), $\{[Ni_2(Htpt)_2(H_2O)_2]\cdot CH_3CN\}_n$ (**5**), $[Ni(H_2tpt)_2]\cdot 3H_2O$ (**6**) based on a multidentate 4-(2,4,6-tricarboxyphenyl)-2,2',6,2"-terpyridine ligand (H_3tpt) have been prepared by hydrothermal synthesis method and structurally characterized. **1**, **2** and **3** show 1-D chain structures, the chains are further linked *via* $\pi\cdot\cdot\pi$ interactions or hydrogen bonds to generate 3-D supramolecular structures. **4** displays a 2-D binodal (3,3)-connected *fes* net with a Schläfli symbol of $(4\cdot 8^2)(4\cdot 8^2)$, which has been reported. **5** also exhibits a 2-D (3,3)-connected *hcb* topology with Schläfli symbol of $(6^3\cdot 6^3)$. **6** is a mononuclear structure. The microbiological properties of **1**-**6** were studied. **1**-**6** showed pretty good antibacterial activities towards *B. subtilis* compared to other bacterial strains. **5** exhibits the smallest MIC value of 1 μg/mL which may be related to the presence of easily-leaving solvent water molecules, thereby exposing more active sites easily.

Keywords: complexes; crystal structure; antibacterial activity

* Corresponding author. E-mail: ljp-zd@zzu.edu.cn

1. Introduction

In the past few years, much interest has been focused on the design and synthesis of coordination polymers not only for their interesting molecular topologies but also for the fact that they exhibit excellent antibacterial activity, which can provide important reference in the design of more efficient antibacterial drugs [1-8]. Factors effecting the antibacterial activity of metal complex are directly related to chelation effect between metal ions and ligands, and the influence of the metal ions on the cell process. The chelation effect reduces the polarity of the metal ions mainly by partial sharing of positive charge with the donor groups and possible π-electron delocalization over the whole chelate rings enhancing the lipophilicity of the complexes [9-10]. This increased lipophilicity may lead to breakdown of the permeability barrier of the cells and thus block the normal cell processes [11]. Earlier articles [12-13] revealed that bidentate or tridentate ligands having more lipophilicity showed higher antimicrobial activity than monodentate ligands, and according to the theory of similarity and intermiscibility, two different types of ligands in complexes have the better antibacterial activity than single ligand. Moreover, another factor affecting the activity is nature of metal ions. Extensively studied transition metals for antimicrobial activity includes silver, copper, nickel, and cobalt complexes, which show different antibacterial properties [14-21]. On the other hand, although complexes with well-defined structure are suitable for exploring the structure-activity relationship, the corresponding reports are limited due to the influence of many complicated factors [22]. It is very important to explore the relationship between the structures of complexes and antibacterial activities, which can provide theoretical guidance for us to design and synthesize complexes with excellent antibacterial activity.

Based on above-mentioned considerations, we selected a terpyridine chelating ligand with multiple aromatic rings named H_3tpt (Scheme 1) to prepare four Cu(II) and two Ni(II) complexes. The antibacterial activities of six complexes were performed against four bacterial strains. Herein, we further explore the relationship

between the structures of six complexes and their biological properties. It should be noted that the structure of **4** has been reported previously [23].

2. Experimental section

2.1 Materials and general methods

The H_3tpt ligand and other reagents were commercially sourced and utilized without further purification. The water used in the experiment was deionized water. Solid UV-vis spectra were obtained in the 200-800 nm range on an Agilent Cary 5000 spectrophotometer. Infrared data for ligand and complexes were measured on a Bruker Tensor 27 infrared spectrometer using a potassium bromide disks in the region of 400-4000 cm^{-1}. Thermogravimetric measurements (TGA, 30~800ºC) were recorded on a Netzsch STA409PC differential thermal analyzer using air atmosphere at a heating rate of 10ºC/min. Elemental analyses (C, H and N) were carried out on a FLASH EA 1112 elemental analyzer. Powder X-ray diffraction (PXRD) was measured on PANalytical X'Pert PRO MPD system.

2.2 Preparation of the complexes

2.2.1 Synthesis of [Cu(Htpt)]$_n$ (1)

Polymer **1** was synthesized hydrothermally in a Teflon-lined stainless steel container by heating a mixture of H_3tpt (8.8 mg, 0.02 mmol), $CuCl_2 \cdot 6H_2O$ (5.1 mg, 0.03 mmol) and 2,2'-bipy (4.7 mg, 0.03 mmol) in 3 mL of H_2O/CH_3CN (1:2) mixed solvent at 130°C for 3 days, and then cooled to room temperature at a rate of 5ºC/h. Blue crystals of **1** were isolated from the filtrate (yield: 60% based on copper). Anal. Calcd for $C_{24}H_{13}CuN_3O_6$: C, 57.26; H, 2.58; N, 8.35. Found: C, 57.36; H, 2.78; N, 8.47%. IR spectra (KBr/pellet, cm^{-1}): 3394m, 1714s, 1604s, 1474s, 1403s, 1347s, 1170m, 1022m, 913w, 800m, 655w, 562w.

2.2.2 Synthesis of {[Cu($H_{1.5}$tpt)$Cl_{0.5}$(H_2O)$_{0.5}$]·1/5H_2O}$_n$ (2)

2 was synthesized by a hydrothermal procedure similar to that described for **1** except using 4,4'-bipy (4.7 mg, 0.03 mmol) instead of 2,2'-bipy. Blue crystals of **2** were isolated from the filtrate. Yield: 73%. Anal. Calcd for $C_{48}H_{29.8}ClCu_2N_6O_{13.4}$: C, 53.95; H, 2.79; N, 7.86. Found: C, 54.15; H, 2.89; N, 7.97%. IR spectra (KBr/pellet, cm^{-1}): 3409s, 3087m, 1714s, 1615s, 1567s, 1472s, 1419s, 1245s, 1112s, 1021m, 912m, 800s, 681m, 455w.

2.2.3 Synthesis of {[Cu(H_2tpt)(H_2O)]·1/2SO_4·2H_2O}$_n$ (3)

A mixture of H_3tpt (8.8 mg, 0.02 mmol), $CuBr_2$ (6.7 mg, 0.03 mmol), H_2O/CH_3CN (1:2, 3 mL) and two drops of concentrated sulfuric acid was sealed in a Teflon-lined stainless steel vessel (25 mL), then heated to 120°C for 72 h, followed by cooling to room temperature at a rate of 5ºC/h. Blue stick crystals of **3** were isolated from the filtrate. The yield of the product **3** was 57%. Anal. Calcd for $C_{48}H_{40}Cu_2N_6O_{22}S$: C, 47.52; H, 3.30; N, 6.93. Found: C, 47.63; H, 3.43; N, 7.04%. IR spectra (KBr/pellet, cm^{-1}): 3428s, 1713s, 1617s, 1557s, 1474s, 1370s, 1325m, 1251m, 1097m, 914w, 798m, 618w, 417w.

2.2.4 Synthesis of [Cu(Htpt)]$_n$ (4)

A mixture of H_3tpt (8.8 mg, 0.02 mmol) and $CuSO_4 \cdot 5H_2O$ (7.5 mg, 0.03 mmol) in solvent of H_2O/DMF (1:2, 3mL) was placed in a 25 mL Teflon-lined stainless steel container, and heated to 130°C for 3 days, then cooled to room temperature. Blue crystals of **4** were isolated from the filtrate (yield: 60% based on copper). The structure of **4** has been reported previously [23].

2.2.5 Synthesis of {[Ni_2(Htpt)$_2$(H_2O)$_2$]·CH_3CN}$_n$ (5) and [Ni(H_2tpt)$_2$]·3H_2O (6)

H_3tpt (8.8 mg, 0.02 mmol), $NiCl_2 \cdot 6H_2O$ (4.8 mg，0.02 mmol) and 3 mL H_2O/CH_3CN (1:2 volume ratio) were mixed in a 25 mL Teflon-lined stainless steel container. The mixture was stirred for 10 min at room temperature and sealed, which was heated at 130°C for 3 days and then slowly cooled to room temperature at the rate of 5°C/h. Finally, blue sheet crystals of **5** (yield: 42% based on nickel) and yellow block crystals of **6** (yield: 26% based on nickel) were isolated from the filtrate and washed by water. Anal.Calcd of crystals **5** for $C_{50}H_{33}N_7Ni_2O_{14}$: C, 55.90; H, 3.07; N, 9.13. Found: C, 55.98; H, 3.12; N, 9.35%. IR spectra (KBr/pellet, cm^{-1}): 3415m, 3069s, 1705s, 1656s, 1601s, 1472s, 1402s, 1348m, 1269s, 1159w, 793s, 680m, 559w, 417w. Anal. Calcd of crystals **6** for $C_{48}H_{34}NiN_6O_{15}$: C, 57.98; H, 3.42; N, 8.45. Found: C, 58.12; H, 3.37; N, 8.65%. IR spectra (KBr/pellet, cm^{-1}): 3415s, 3065s, 1710s, 1601s, 1570m, 1551m, 1469w, 1423m, 1247s, 1164m, 1015w, 916w, 793w, 768w, 691w.

2.3 Crystal structure determination

X-ray diffraction data were collected with a Bruker APEXII CCD diffractometer at temperature of 298 ± 1K using Mo-*Kα* ray (λ=0.71073 Å) for **1**-**2**, **5**-**6** and Cu-*Kα* ray (λ=1.5418 Å) for **3** and **4**. All crystal structures were solved by direct methods with the SHELXS-97 crystallographic software package [24]. Crystal structures of **2**, **3**, **4**, **6** were refined by full-matrix least-squares technique based on F^2 with the SHELXL-2014 crystallographic software package [25]. The structures of **1** and **5** were first refined with the SHELXL-2015 crystallographic software package [26]. Finally, the structures of **1** and **5** were refined with Olex 2 crystallographic software package [27]. The data of **1**, **2**, **4**, **5** were corrected with SQUEEZE to remove the solvent molecules due to severe crystallographic disorder [28]. All atoms were refined anisotropically except hydrogen atoms. A summary of the crystallographic data and processing parameters is presented in Table 1 and Table 2. Table S1 show selected bond lengths and angles of **1**-**6**.

2.4 Antibacterial activity

To measure bacteriostatic activities of **1**-**6** and ligand against Gram-positive *Bacillus subtilis* CMCC(B) 63501, *Staphylococcus aureus* ATCC 29213, Gram-negative *Escherichia coli* ATCC 25922, *Salmonella enteritidis* ATCC 13076, inhibition zone were performed using the agar diffusion technique [29-30]. The nutrient agar medium and 6mm diameter paper discs were used. DMSO was used as solvent to dissolve the compounds and also used as control. The filter paper discs were soaked in different solution of the compounds and then placed in the Petri dishes previously seeded with the test organisms. The experiment for each compound has been done in triplicate. The plates were incubated for 18 hours at 37^{o}C and the inhibition zone around each disc was measured in mm using vernier caliper. The average zone of inhibition in millimeter was determined from the readings taken in triplicate (Table 3). Typical inhibition zones of obtained complexes **1**(a), **3**(b), **5**(c), **6**(d) against B. subtilis are shown in Fig. S1. Activity was determined by measuring the diameter of the zone of inhibition in mm. An inhibition zone diameter over 7 mm indicates that the tested compound is active against the bacteria under investigation. From the results of the inhibition zone experiments, it is found that all complexes inhibit *Bacillus subtilis*, whereas no compounds show obvious inhibitory effect towards *E. coli*, *S. aureus*, *S. enteritidis*. Therefore, the minimum inhibitory concentration (MIC) of **1**-**6** for *Bacillus subtilis* was conducted using agar dilution methods [11]. MIC was the minimum sample concentration that completely inhibited the growth of bacteria in the pores [31]. Each compound was dissolved in DMSO at different concentrations of 128, 64, 32, 16, 8, 4, 2, 1, 0.5 μg/mL. A preculture of *Bacillus subtilis* was grown in LB (Luria Broth) for 18 h at the most favorable temperature. This culture was used as a control to examine if the growth of bacteria tested is normal. In a similar second culture, 100 μL of the bacteria as well as DMSO at the desired concentration were added. The MIC endpoint is the lowest concentration of complex that produces inhibition of bacterial growth. In addition,

two percent of DMSO without active ingredients was used as a positive control to assess the MIC values of the strains. Kanamycin, Gatifloxacin, Norfloxacin, Ciprofloxacin, Sparfloxacin and Streptomycin served as standard bactericides [5,12,32-33]. The MIC values for all complexes and representative commercial antibiotics are expressed as μg/mL in Table 4.

3. Results and Discussion

3.1 Structural description of [Cu(Htpt)]$_n$ (1)

Crystal data of the compound reveals that **1** crystallizes in the triclinic system, *P*-1 space group, which exhibits one dimensional double-chain structure. The asymmetric unit of **1** possesses one crystallographically unique Cu(II) cation, one $Htpt^{2-}$ ligand. As shown in Fig. 1a, each five-coordinated Cu(II) ion is in a slightly distorted square-pyramidal environment with a Addison trigonality factor τ=0.269 [34]. The Cu(II) ion is coordinated by three nitrogen atoms [Cu1-N1A: 2.014(4) Å, Cu1-N2A: 1.941(3) Å, Cu1-N3A: 2.034(4) Å] and two oxygen atoms [Cu1-O2: 2.230(4) Å, Cu1-O6B: 1.926(3) Å] (Scheme 2a). The oxygen atoms (O3, O4) of the carboxylate groups in **1** are disordered. The surrounding bond angles of **1** are shown in Table S1. The bond lengths and bond angles around Cu(II) ion are in the normal range [35-36]. The $Htpt^{2-}$ ligands connect neighboring Cu(II) ions by N/O chelation to yield limitless 1-D double chains (Fig. 1b). As shown in Fig. 1c, adjacent parallel 1-D double chains form a 2-D supramolecular layer through $\pi\cdots\pi$ interactions between pyridine rings (average face-to-face distances of 3.484(1) Å, and centroid-to-centroid distances of 3.996(6) Å) [37-38]. Additionally, the 2-D layers are further bridged through the weaker C-H$\cdots$O hydrogen bonds in **1** {H/O distances (bond angles): 2.180(4) Å [143.23(1)^o] for C4-H4$\cdots$O5, 2.638 Å (123.01^o) for C9-H9$\cdots$O4} along *a* direction. They are in the normal range of C-H$\cdots$O hydrogen bonds [39-40]. The 2D planar structure is further stacked into a 3-D supramolecular structure by another $\pi\cdots\pi$ interaction between inter-molecular pyridine rings [interplanar separations: 3.355(2)

Å; centroid-centroid separations: 3.524(4) Å]. Both the above interactions extend the above 1-D double chains into 3-D supramolecular structure.

3.2 Structural description of {[Cu($H_{1.5}$tpt)$Cl_{0.5}$(H_2O)$_{0.5}$]·1/5H_2O}$_n$ (2)

Single-crystal X-ray diffraction analysis reveals that **2** is a 1-D structure and crystallizes in the triclinic crystal system, space group *P*-1. The asymmetric unit of **2** possesses one crystallographically unique Cu(II) cations, one $H_{1.5}tpt^{1.5-}$ ligand including a H5 and half a H2, half a Cl^- anion and half a coordinated water molecule located in the same coordination site, 1/5 lattice water molecule. The disorder occurs on the oxygen atoms and chlorine atoms (O6, Cl1, O8) in **2**. As shown in Fig. 2a, each Cu(II) ion is five-coordinated with a slightly distorted square-pyramidal environment (τ=0.0833) involving three nitrogen atoms (N1, N2, N3), one oxygen atoms (O3A) from the $H_{1.5}tpt^{1.5-}$ ligand, half a coordinated Cl atom (Cl1) and half an oxygen atoms (O8) located in the same coordination site (Scheme 2b). The bond lengths of Cu-O3A and Cu-O8 are 1.941(1) and 2.194(2) Å and the Cu-N bond lengths are 1.942(1), 2.040(2) and 2.041(1) Å, respectively. The bond length of Cu-Cl1 is 2.586(3) Å. The above bond lengths are within the range reported for square-pyramidal environments [41]. The surrounding bond angles of Cu(II) are shown in Table S1. They are in the normal range [41]. Neighboring Cu(II) ions are linked to form a 1-D single chain through $H_{1.5}tpt^{1.5-}$ ligands. Furthermore, these 1-D chains are assembled together by C-H···O hydrogen bonds {H/O distances (bond angles) 2.470(3) Å [137.939(1)^o] for C3-H3···O4} to form a 2-D layer (Fig. 2b). The 2-D layers are further outspread to 3-D structure by the intermolecular C-H···O hydrogen bonds (Fig. 2c) {H/O distances (bond angles): 2.599(9) Å [161.333(1)^o] for C9-H9···O5}, which agree well with those reported in the literature [42-43].

3.3 Structural description of {[Cu(H_2tpt)(H_2O)]·1/2SO_4·2H_2O}$_n$ (3) and [Cu(Htpt)]$_n$ (4)

The crystal data shows that **3** crystallizes in the orthorhombic crystal lattice with space group *Pbcn*. As shown in Fig. 3a, **3** consists of one Cu(II) ion, one H_2tpt^- ligand, one coordinated water molecule, half a SO_4^{2-} anion and two lattice water molecules. Each Cu(II) ion is five-coordinated to form a slightly distorted square-pyramidal geometry (τ=0.031). One oxygen donors (O4A) from the other H_2tpt^- ligand, an oxygen donor (O11) of the water molecule and three nitrogen donors (N2, N3, N5) of the pyridine from the ligand are coordinated with the Cu(II) ion (Scheme 2c). The bond distances of Cu1-N2, Cu1-N3, and Cu1-N5 are 2.045(3), 2.036(3), 1.936(2) Å while the bond lengths of Cu1-O4A and Cu1-O11 are 1.934(2), 2.244(3) Å, respectively (Table S1). They are in the normal range [44-45]. In **3**, the Cu(II) ions are connected by H_2tpt^- ligand to give rise to a 1-D zigzag chain in the *ab* plane, in which the Cu1···Cu1 distance is 7.895(1) Å (Fig. 3b). Moreover, two types of π··π stacking interactions can be seen in **3**. One is between adjacent pyridine rings with a centroid-to-centroid distance of 3.670(2) Å and face-to-face distance of 3.400(0) Å, which give rise to a 2-D infinite packing structure (Fig. 3c); the other is between neighboring benzene rings with a centroid-to-centroid distance of 3.854(2) Å and face-to-face distance is 3.370(1) Å, which further extend the 2-D structure into a 3-D supramolecular architecture.

Single-crystal X-ray diffraction reveals that **4** is a two-dimensional structure and crystallizes in monoclinic system with space group $P2_1/n$. It should be noted the structure of **4** has been reported previously [23]. Hence, the description of the crystal structure is omitted.

3.4 Structural description of $\{[Ni_2(Htpt)_2(H_2O)_2]\cdot CH_3CN\}_n$ (5)

The crystal data shows that **5** is the monoclinic system, $P2_1/c$ space group. As illustrated in Fig. 4a, the independent unit of **5** is composed of two similar-coordinated Ni(II) cations, two $Htpt^{2-}$ ligands, two coordinated water molecules, one lattice CH_3CN molecule. The O11 and O12 atoms of carboxylate groups in **5** present disordered state. Both Ni1 and Ni2 in distorted octahedron

geometries are coordinated by three nitrogen atoms and three oxygen atoms. In Ni1, one equatorial coordination site is occupied by N1, N2, N3 from $Htpt^{2-}$ ligand and O13 from one coordinated water molecule (Scheme 2a). The apical position is occupied by O4B and O7C from two $Htpt^{2-}$ ligands. Similar to Ni1, Ni2 is coordinated by three nitrogen atoms (N4, N5, N6) from $Htpt^{2-}$ ligand adopting chelating coordination and an oxygen atom (O14) from coordinated water molecule at the equatorial positions. In addition, Ni2 is coordinated by two other oxygen atoms (O11A, O1) from two $Htpt^{2-}$ ligands in monodentate mode at the axial positions. The bond distances of Ni1-N1, Ni1-N2, Ni1-N3 are 1.948(5), 2.074(7), 2.050(7) Å, and the Ni1-O13 is 1.987(5) Å, Ni1-O7C is 2.059(6) Å, Ni1-O4B is 2.025(6) Å. The bond distances of Ni2-N4, Ni2-N5, Ni2-N6 are 1.956(5), 2.079(7), 2.054(7) Å, and the Ni2-O1 is 2.033(5) Å, Ni2-O11A is 2.059(1) Å, Ni2-O14 is 1.992(5) Å. The bond angles around Ni(II) ion are shown in Table S1. They are in the normal range [46]. In **5**, adjacent Ni(II) atoms are connected through $Htpt^{2-}$ ligand adopting chelating mode to give rise to 1-D zigzag chain which Ni1···Ni2 distance is 13.160(7) Å. The 1-D zigzag chains are further linked by the carboxyl oxygen atoms of $Htpt^{2-}$ ligands to form a 2-D planar structure in which the adjacent Ni1···Ni1 distance is 8.976(0) Å (Fig. 4b).

For achieving further insight into the structure of **5**, we can simplify $Htpt^{2-}$ ligands and Ni(II) ions from the topological point of view. The structure of **5** is binodal with three-connected [Ni(II) ion] and three-connected ($Htpt^{2-}$ ligands) nodes, and exhibits a fascinating 2-D topology network (Fig. 4c). Thus, the overall structure of **5** can be described as a (3,3)-connected *hcb* net with a Schläfli symbol of $(6^3 \cdot 6^3)$ calculated by the TOPOS program [47-49].

3.5 Structural description of $[Ni(H_2tpt)_2]\cdot 3H_2O$ (6)

Single-crystal X-ray diffraction analysis reveals that **6** crystallizes in the monoclinic system, $P2_1/c$ space group. The independent unit of **6** contains one Ni(II) ion, two H_2tpt^- ligands and three lattice water molecules. It should be pointed out that

the disorder occurs on the oxygen atoms (O1, O2, O7, O8) of carboxylate groups. The six-coordinated Ni(II) ion is in a distorted octahedral environment involving four nitrogen atoms (N2, N4, N5, N6) from two ligands at the equatorial positions and two nitrogen atoms (N1, N3) at the axial positions (Scheme 2d). The bond lengths of Ni1-N1, Ni1-N2, Ni1-N3, Ni1-N4, Ni1-N5, Ni1-N6 are 2.098(2), 1.988(2), 2.097(3), 1.984(2), 2.132(2), 2.120(2) Å, respectively. And the bond angles around Ni(II) are shown in Table S1. They are consistent with the reported Ni(II) complexes [50-51]. As illustrated in Fig. 5a, six terpyridyl nitrogen atoms from two H_2tpt^- ligands connect one Ni(II) ion to form $[Ni(Htpt)_2]$ molecule. The adjacent $[Ni(Htpt)_2]$ molecules form 2-D structure through the stronger C-H···O hydrogenbonds in the *ac* plane (Fig. 5b). The H···O distances (bond angles) of the O-H···O hydrogen bonds are 2.496(5) Å [128.507(1)°] for C19A-H1A···O11, 2.364(5) Å [155.795(5)°] for C38-H38···O9. Moreover, adjacent 2-D layers are further connected by C-H···O hydrogen bonds {H/O distances (bond angles): 2.353(5) Å [148.827(2)º] for C16-H16···O3; 2.383(5) Å [148.431(4)º] for C22-H22···O2} to form 3-D supramolecular structure in the *bc* plane. The lengths of C-H···O hydrogen bonds agreewell with those reported in the literatures [52-54].

The PXRD patterns of **5** and **6** are shown in Figure S2. It could be seen that result of the most peak positions was concordant to the simulated from single crystal data, indicating that the synthesized complexes possess high phase purity.

3.6 UV/vis absorbance properties and IR spectroscopy

The solid-state UV-vis absorption spectroscopy of complexes **1**-**3**, **5**-**6** and H_3tpt ligand have been studied (Fig. S3). It is obvious that the H_3tpt ligand shows the absorption band around 335 nm, which can be assigned to the intraligand π-π* transition. Similarly, all complexes show weak shoulder band around 335 nm, which suggest that the coordination of the metal ions hardly alters the intrinsic electronic properties of the H_3tpt ligand [55-56]. Compared to the H_3tpt ligand, all the Cu(II) complexes display similar spectral feature containing a broad absorption band around

686 nm. The absorption band of **5** in the vision region was observed at ca. 618 nm. These bands in the absorption spectra can be attributed to the d-d transition of the Cu(II) and Ni(II) [55-56].

The IR spectra of H_3tpt ligand, **1**-**3** and **5**-**6** are shown in Fig. S4. The vibrational bands present at 3410 and 3094 cm^{-1} should be ascribed to the ν(O-H) and ν(C-H) in ligand. The bands around 3400 cm^{-1} in complexes could be attributed to the ν(O-H) of the carboxyl groups, which indicates carboxyl groups in complexes are not fully involved in the coordination. The bands of H_3tpt at 1712 cm^{-1} and 1597 cm^{-1} are attributed to the stretching vibration of the C=O bonds of carboxyl groups and C=N bonds of the pyridine rings. The characteristic shifting bands of ν(C=O) and ν(C=N) (shown in Table S2) in complexes is indicative of the coordination state between the central ions and H_3tpt. The absorption peaks in the range of 1112-1269 cm^{-1} are assigned to C-O stretching vibrations for H_3tpt and the complexes. In addition, in all complexes, strong bands observed in the range of 1601-1656 cm^{-1} are associated with asymmetric stretching vibrations $\nu(COO^-)_{as}$ of the carboxylic acid groups, while the peaks in the range of 1347-1423 cm^{-1} are attributed to symmetric stretching vibrations $\nu(COO^-)_s$ of the carboxylic acid groups [57-59].

3.7 Thermogravimetric analysis

The thermal properties of **1**-**3**, **5**-**6** were characterized by thermogravimetric analysis (TGA) (Figure S5). The metal coordination complexes were heated in a temperature range of 30-800°C in an air atmosphere. The thermal decomposition of as-prepared complexes proceeds with two degradation steps. The first step of decomposition can be attributed to the loss of solvent molecules at 50-200°C for **1** and at 30-200°C for **5**, and the loss of lattice water molecules, coordinated water molecules, and coordinated Cl ions at 135-205°C for **2**. As for **3** and **6**, the first step of weight loss at 80-235°C and 70-180°C corresponds to the loss of lattice water molecules. The second decomposition stage involves the removal of the ligand, resulting in the collapse of the crystal structure. For **1**-**3**, the residue is CuO with

weight loss of 86.29% (Calcd. 84.18%), 84.87% (Calcd. 85.09%), 83.55% (Calcd. 86.87%), respectively. As for **5**-**6**, the total weight loss amounts to 89.79% (Calcd. 93.04%), 89.86% (Calcd. 92.48%) leaving NiO as a residue. Table S3 reports the calculated and experimental weight losses, and the temperature range of decomposition for these complexes studied.

3.8 Antibacterial activity

The search for agents with antibacterial activity is an important field of research nowadays. Many researchers have reported the antibacterial activity of complexes due to various molecular architectures and different metal center of complexes [60-61,12,13]. In this work, from an insight of coordination chemistry, **1**-**6** containing same ligand are suitable for the research of antibacterial mechanism and the structure-function relationship. Herein, antibacterial activity of as-prepared **1**-**6** and H_3tpt ligand against two Gram(+) bacterial strains [*Bacillus subtilis* CMCC(B) 63501, *Staphylococcus aureus* ATCC 29213] and two Gram(−) bacterial strains (*Escherichia coli* ATCC 25922, *Salmonella enteritidis* ATCC 13076) was studied using the method of the agar diffusion technique. As shown in Table 3, the diameters of inhibition zones for **1**-**6** against *B. subtilis* are obviously larger than those of other bacterial strains, which shows that all complexes demonstrate selective antibacterial activity. Compared to the metallic salt and the corresponding ligands, all complexes show antibacterial activity towards *B. subtilis*, which can be attributed to the chelation theory where chelation of metal ions and ligands reduces the polarity of the metal ion mainly because of partial sharing of its positive charge with the donor groups and possible π-electron delocalization within the whole chelate ring [62-67]. Furthermore, according to the theory of similarity and intermiscibility, the chelate process improves lipophicity of central metal, which subsequently favours its permeation through the lipid layer of cell membranes and further inhibit enzyme activity, which resulting in excellent antibacterial activity [68-70].

In order to further compare their antimicrobial activities, **1**-**6** were selected against

B. subtilis for minimum inhibitory concentration (MIC) studies. As present in Table 4, compared with other copper complexes, **3** shows the excellent antibacterial performance with an MIC value of 2 μg/mL. Analyzing from the structure, **3** contains easily-leaving coordinated water molecules, thereby exposing more active sites easily, which may be an important factor exhibiting excellent antibacterial activity. Similarly, compared with **6**, **5** also exhibit outstanding activity because **5** has also easily-leaving coordinated water molecule. Furthermore, the difference of metal ion may be one of the reasons why **5** exhibits the higher antimicrobial activity than **3**. In contrast, **6** showed weaker antibacterial activity compared to other complexes. This is probably due to the fact that Ni(II) is coordinated by terpyridyl nitrogen atoms of two H_3tpt ligands adopting bis-tridentate chelating coordination mode, thus it is difficult to expose the active site because of its stable structure. Our results preliminary reveal that the antibacterial activities are related to complex structures. Namely, containing easily-leaving coordinated water molecules in as-prepared complexes, thereby exposing more active sites easily, is an important factor exhibiting excellent antibacterial activity.

4. Conclusion

In summary, four Cu(II) complexes and two Ni(II) complexes based on H_3tpt ligand have been synthesized and characterized. Thermogravimetric analysis has been used to determine the structural stability, which shows that the thermal decomposition results in the metal oxides as residues. The antibacterial activities of as-prepared **1**-**6** against four strains have been studied, which reveals all complexes show selective antibacterial activity against *B. subtilis*. Our study on antimicrobial activity demonstrates that the complexes containing easily-leaving coordinated water molecules exhibit excellent antibacterial activity. This work preliminarily reveals that the antibacterial activities are related to complex structures. The mode of action and antibacterial mechanism still need further exploration and validation.

Acknowledgment:

We are thankful for financial support from National Natural Science Foundation of China (Nos. J1210060), Science and technology research program of Henan Province of China (162102210167, 172102210483), Key scientific research projects of Henan Province of China (17A150020), Natural Science Foundation of Henan Province of China (182300410216), National Undergraduate Innovation and entrepreneurship training project (201810459007), College Science and Technology Innovation Team of Henan Province (Nos. 16IRTSTHN001) and the Science & Technology Innovation Talent Plan of Henan Province (Nos. 174200510018).

Appendix A. Supplementary data

Crystallographic data for the structures reported in this paper have been deposited with the Cambridge Crystallographic Data Centre as supplementary publication with CCDC numbers 1861713-1861715 (**1**-**3**) and 1861716-1861717 (**5**-**6**). Copies of the data can be obtained free of charge on application to CCDC, 12 Union Road, Cambridge CB2 1EZ, UK (fax: (44) 1223 336-033; e-mail: deposit@ccdc.cam.ac.uk).

REFERENCES

[1] I. R. Colinas, M. D. Rojas-Andrade, I. Chakraborty, S. R. J. Oliver, CrystEngComm, 20 (2018) 3353.

[2] N. M. Urquiza, M. S. Islas, M. L. Dittler, Inorg. Chim. Acta, 405 (2013) 243.

[3] M. Montazerozohori, S. Yadegari, A. Naghiha, J. Serb. Chem. Soc., 79 (2014) 793.

[4] L. Liu, C. H. Liu, L. Nie, T. Jiang, J. Hong, X. M. Zhang, L. H. Luo, X. L. Wang, Inorg. Chim. Acta, 435 (2015) 66.

[5] M. Salehi, F. Rahimifar, M. Kubicki, A. Asadi, Inorg. Chim. Acta, 443 (2016) 28.

[6] Z. H. Chohan, M. M. Naseer, Appl. Organomet. Chem., 21 (2007) 1005.

[7] X. Y. Wu, H. X. Qi, J. J. Ning, J. F. Wang, Z. G. Ren, J. P. Lang, Appl. Catal. B Environ., 168 (2015) 98.

[8] F. L. Yuan, Y. Q. Yuan, M. Y. Chao, D. J. Young, W. H. Zhang, J. P. Lang, Inorg. Chem., 56 (2017) 6522.

[9] Y. P. Hao, C. P. Yue, B. N. Jin, Y. L. Lv, Q. K. Zhang, J. P. Li, Z. Y. Liu, Polyhedron, 139 (2017) 296.

[10] Q. K. Zhang, C. P. Yue, Y. Zhang, Y. L. Lv, Y. P. Hao, Y. L. Miao, J. P. Li, Z. Y. Liu, Inorg. Chim. Acta, 473 (2018) 112.

[11] M. K. Paira, T. K. Mondal, D. Ojha, A. M. Z. Slawin, E. R. T. Tiekink, A. Samanta, C. Sinha, Inorg. Chim. Acta, 370 (2011) 175.

[12] M. N. Patel, P. A. Dosi, B. S. Bhatt, Polyhedron, 29 (2010) 3238.

[13] G. Psomas, C. D. Samara, P. Philippakopoulos, V. Tangoulis, C. P. Raptopoulou, E. Samaras, D. P. Kessissoglou, Inorg. Chim. Acta, 272 (1998) 24.

[14] S. M. Abdallah, G. G. Mohamed, M. A. Zayed, M. S. Abou El-Ela, Spectrochim. Acta, Part A, 73 (2009) 833.

[15] S. M. Abdallah, M. A. Zayed, G. G. Mohamed, Arabian J. Chem., 3 (2010) 103.

[16] S. J. Sabounchei, F. B. Akhlaghi, Z. Mozafari, C. Boskovic, R. W. Gable, R. Karamian, M. Asadbegy, Dalton Trans., 42 (2013) 2520.

[17] T. Palacios-Hernández, H. Höpfl, J. L. Sánchez-Salas, E. González-Vergara, A. Pérez-Benítez, M. A. Quiroz-Alfaro, M. A. Méndez-Rojas, J. Inorg. Biochem., 139 (2014) 85.

[18] M. N. Patel, A. P. Patidar, Monatsh. Chem. 145 (2014) 369.

[19] G. M. Bobiev, T. D. Sufiev, A. N. Shakhmatov, Pharm. Chem. J., 42 (2008) 614.

[20] F. Wang, Y. T. Wang, H. Yu, J. X. Chen, B. B. Gao, J. P. Lang, Inorg. Chem., 55 (2016) 9417.

[21] F. L. Hu, Y. Mi, C. Zhu, B. F. Abrahams, P. Braunstein, J. P. Lang, Angew. Chem. Int. Ed., 57 (2018) 12696.

[22] K. Ghazal, S. Shoaib, M. Khan, S. Khan, M. K. Rauf, N. Khan, A. Badshah, M. N. Tahir, I. Ali, A. Rehman, J. Mol. Struct., 1177 (2019) 124.

[23] E. J. Gao, Y. H. Feng, J. Q. Su, B. Meng, B. Jia, Z. Z. Qi, T. T. Peng, M. C. Zhu, Appl. Organomet. Chem., 32 (2018) e4164.

[24] G. M. Sheldrick, SHELXS-97: Programs for X-ray Crystal Structure Solution; University of

Göttingen: Göttingen, Germany, 1997.

[25] G. M. Sheldrick, Acta Cryst. A64 (2008) 112.

[26] G. M. Sheldrick. Acta Cryst. C71 (2015) 3.

[27] O. V. Dolomanov, L. J. Bourhis, R. J. Gildea, J. A. K. Howard, H. Puschmann, J. Appl. Cryst., 42 (2009) 339.

[28] A. L. Spek, Acta Cryst., C71 (2015) 9.

[29] A. C. Tella, J. A. Obaleye, Orbital Elec. J. Chem. 2 (2010) 11.

[30] P. Raj, A. Singh, A. Singh, N. Singh. ACS Sustainable Chem. Eng., 5 (2017), 6070.

[31] Y Göka, S Akkoçb, S Albayrakc, M Akkurtd, M. N. Tahire, Appl. Organomet. Chem., 28 (2014) 244.

[32] K. R. Surati, Spectrochim. Acta, Part A, 79 (2011) 272.

[33] A. F. Elhusseiny, A. Eldissouky, A. M. Al-Hamza, J. Mol. Struct., 1100 (2015) 530.

[34] A. W. Addison, T. N. Rao, J. Reedijk, V. R. Jacobus, G. C. Verschoor, J. Chem. Soc. Dalton Trans., 1984, 1349.

[35] Y. Q. Duan, J. H. Huang, S. C. Liu, T. T. Yu, J. P. Li, Y. P. Hao, Z. Y. Liu, B. Liu, Inorg. Chem. Commun., 81(2017) 47.

[36] B. L. Liu, J. Dang, S. Q. Zang, Y. X. Wang, R. J. Tao, Inorg. Chem. Commun., 14 (2011) 31.

[37] J. C. Li, H. X. Li, H. Y. Li, W. J. Gong, J. P. Lang, Cryst. Growth Des., 16 (2016) 1617.

[38] Y. X. Shi, W. X. Li, W. H. Zhang, J. P. Lang, Inorg. Chem., 57 (2018) 8627.

[39] J. P. Li, B. J. Li, M. T. Pan, B. Liu, J. J. Cheng, R. Y. Li, X. L. Gao, S. M. Wang, H. W. Hou, Z. Y. Liu. Cryst. Growth Des., 17 (2017), 2975.

[40] F. L. Li, Q. Shao, X. Q. Huang, J. P. Lang, Angew. Chem. Int. Ed., 57 (2018) 1888.

[41] M. A. Hossain, C. Y. L. Low, C. M. Sheikh, J. C. Juan, H. VoonLee, J. Mol. Struct., 1175 (2019) 566.

[42] C. D. Zhang, S. X. Liu, C. Y. Sun, F. J. Ma, Z. M. Su, Cryst. Growth Des., 9 (2009) 3655.

[43] B. Wu, W. H. Zhang, Z. G. Ren, J. P. Lang, Chem. Commun., 51 (2015) 14893.

[44] J. J. Cheng, S. M. Wang, Z. Shi, H. Sun, B. J. Li, M. M. Wang, M. Y. Li, J. P. Li, Z. Y. Liu, Inorg. Chim. Acta, 453 (2016) 86.

[45] Z. Q. Xu, Q. Wang, H. J. Li, W. Meng, Y. Han, H. W. Hou, Y. T. Fan. Chem. Commun., 48 (2012) 5736.

[46] B. Li, M. M. Dong, H. T. Fan, C. Q. Feng, S. Q. Zang, L. Y. Wang, Cryst. Growth Des., 14 (2014) 6325.

[47] V. A. Blatov, IUCr, Comput. Comm. Newslett., 7 (2006) 4.

[48] V. A. Blatov, TOPOS, A multipurpose crystallochemical analysis with the program package, Samara State University, Samara, Russia, 2009.

[49] A. Schoedel, A. J. Cairns, Y. Belmabkhout, L. Wojtas, M. Mohamed, Z. Zhang, D. M. Proserpio, M. Eddaoudi, M. J. Zaworotko, Angew. Chem. Int. Ed., 52 (2013) 2902.

[50] L. A. Guo, C. Huang, L. Liu, Z. C. Shao, Y. Tong, H. W. Hou, Y. T. Fan, Cryst. Growth Des., 16 (2016) 4926.

[51] X. Y. Duan, M. L. Wei, Cryst. Growth Des., 17 (2017) 1197.

[52] C. L. Zhou, S. M. Wang, S. N. Liu, T. T. Yu, R. Y. Li, H. Xu, Z. Y. Liu, H. Sun, J. J. Cheng, J. P. Li, H. W. Hou, J. B. Chang. J. Mol. Struct., 1118 (2016) 139.

[53] Z. M. Ju, W. Yan, X. J. Gao, Z. Z. Shi, T. Wang, H. G. Zheng, Cryst. Growth Des., 16 (2016) 2496.

[54] F. Wang, F. L. Li, M. M. Xu, H. Yu, J. G. Zhang, H. T. Xia, J. P. Lang, J. Mater. Chem. A, 3 (2015) 5908.

[55] M. M. Dong, L. L. He, Y. J. Fan, S. Q. Zang, H. W, Hou, T. C. W. Mak, Cryst. Growth Des., 13 (2013) 3353.

[56] L. Liu, C. Huang, X. N. Xue, M. Li, H. W. Hou, Y. T. Fan, Cryst. Growth Des., 15 (2015) 4507.

[57] A. C. Kathalikkattil, K. K. Bisht, N. Aliaga-Alcalde, E. Suresh. Cryst. Growth Des., 11 (2011) 1631.

[58] L. L. Yu, X. M. Wang, M. L. Cheng, H. R. Rong, Y. D. Song, Q. Liu, Cryst. Growth Des., 18 (2018) 280.

[59] M. S. Khana, M. Khalid, M. S. Ahmad, M. Ahmad, M. Ashafaq, Rahisuddin, R. Arif, M. Shahid, J. Mol. Struct., 1175 (2019) 889.

[60] Z. H. Chohan, Appl. Organomet. Chem., 20 (2006) 112.

[61] Z. H. Chohan, M. Arif, Z. Shafiq, M. Yaqub, C. T. Supuran, J. Enzyme Inhib. Med. Chem., 21 (2006) 95.

[62] A. Z. El-Sonbati, M. A. Diab, S. M. Morgan, A. M. Eldesoky, M. Z. Balboula, Appl.

Organometal. Chem., 32 (2018) e4207.

[63] A. Z. El-Sonbati, A. A. El-Bindary, G. G. Mohamed, S. M. Morgan, W. M. I. Hassan, A. K. Elkholy, J. Mol. Liq., 218 (2016) 16.

[64] M. A. Diab, A. Z. El-Sonbati, Sh. M. Morgan, M. A. El-Mogazy, Appl. Organometal. Chem., 32 (2018) e4378.

[65] R. P. Ye, J. X. Yang, X. Zhang, L. Zhang, Y. G. Yao, J. Mol. Struct., 1106 (2016) 192.

[66] L. Tabrizi, P. McArdle, M. Ektefan, H. Chiniforoshan, Inorg. Chim. Acta, 439 (2016) 138.

[67] N. Dharmaraj, P. Viswanathamurthi, K. Natarajan, Transition Met. Chem., 26 (2001) 105.

[68] D. P. Singh, V. Malik, K. Kumar, C. Sharma, K. R. Aneja, Spectrochim. Acta A, 76 (2010) 45.

[69] A. Caudhary, R. V. Singh, Phosphorus Sulfur Silicon Relat. Elem., 178 (2003) 603.

[70] W. H. Mahmoud, R. G. Deghadi, G. G. Mohamed, Appl. Organometal. Chem., 30 (2016) 221.

Captions:

Scheme 1. Structure of the H_3tpt ligand.

Scheme 2. (a) Coordination modes found in **1** and **5**. (b) Coordination modes found in **2**. (c) Coordination modes found in **3**. (d) Coordination modes found in **6**.

Table 1. Crystallographic data for **1**-**3**.

Table 2. Crystallographic data for **4**-**6**.

Table 3. Antimicrobial screening results of the H_3tpt ligands, **1**-**6** and metal salts.

Table 4. Minimum inhibition concentration (MIC) values for **1**-**6** and some standard drugs.

Table S1. Selected bond distances (Å) and bond angles (deg) for **1**-**6**.

Table S2. Selected IR frequencies of the H_3tpt, **1**-**3** and **5**-**6**.

Table S3: Theoretical & experimental weight loss of the complexes.

Figure S1. Typical inhibition zones of complexes **1**(a), **3**(b), **5**(c), **6**(d) against B. subtilis.

Figure S2. PXRD patterns for as-synthesized **5** and **6**.

Figure S3. UV-vis absorption spectra at room temperature for the free the H_3tpt, **1**-**3** and **5**-**6**.

Figure S4. IR spectra of as-prepared complexes and the free ligand.

Figure S5. The TG curves for **1**-**3**, **5**-**6**.

Figure 1. (a) The coordination environment of Cu(II) atom in **1** (A: 1-x, -y-1, -z+2; B: 2-x, -1-y, 3-z), all hydrogen atoms are omitted for clarity. (b) The 1-D double chains structure. (c) 2-D structure resulting from π···π stacking.

Figure 2. (a) The coordination environment of Cu(II) atom in **2** (A: x, y, z+1), part of the hydrogen atom is omitted for clarity. (b) The 2-D supramolecular network. (c) 3-D supramolecular structure constructed by hydrogen-bonding interactions.

Figure 3. (a) The coordination environment of Cu(II) atom in **3** (A: -x+3/2, y-1/2, z), all hydrogen atoms are omitted for clarity. (b) The 1-D zigzag chains structure. (c) 2-D structure resulting from π···π stacking.

Figure 4. (a) The coordination environment of Ni(II) atom in **5** (A: x, -y+1/2, z+1/2; B: -1+x, -y+1/2, z-1/2), all hydrogen atoms are omitted for clarity. (b) The 2-D planar network. (c) Views of topology of **5** [The blue balls represent Ni(II) atoms, the pink balls represent the $Htpt^{2-}$ ligands, respectively].

Figure 5. (a) The coordination environment of Ni(II) atom in **6**, all hydrogen atoms are omitted for clarity. (b) 2-D structure resulting from C-H···O hydrogen-bonding interactions.

Table 1. Crystallographic data for **1-3**.

Complexes	**1**	**2**	**3**
Formula	$C_{24}H_{13}CuN_3O_6$	$C_{48}H_{29.8}ClCu_2N_6O_{13.4}$	$C_{48}H_{40}Cu_2N_6O_{22}S$
Fw	502.91	1067.51	1212.00
Temperature(K)	293(2)	293(2)	273(2)
Wavelength(Å)	0.71073	0.71073	1.54178
Crystal system	triclinic	triclinic	rthorhombic
Space group	*P*-1	*P*-1	*Pbcn*
a(Å)	9.2864(14)	8.1583(16)	25.5176(5)
b(Å)	10.9212(16)	11.151(2)	13.9277(3)
c(Å)	12.1185(18)	12.752(3)	13.5555(3)
α(deg)	112.949(3)	77.00(3)	90
β(deg)	107.104(3)	76.20(3)	90
γ(deg)	94.009(4)	85.53(3)	90
V(Å^3)	1057.7(3)	1097.4(4)	4817.65(18)
Z	2	1	4
D_c(g·cm^{-3})	1.579	1.615	1.671
F(000)	510	542	2480
θ range for data collection(deg)	3.36~28.460	3.367~27.103	3.464~68.424
Reflections collected /unique	30315/5326	43225/4843	51354/4435
Data/restraints/ params	5326/3/314	4843/14/346	4435/7/359
Goodness-of-fit on F^2	1.080	1.044	1.052
Absorption coefficient	1.081	1.108	2.323
Tmin/Tmax	0.6871, 0.7457	0.6933, 0.7455	0.6478, 0.7531
Final R1[a], wR2[b]	0.0819, 0.1429	0.0399, 0.1106	0.0490, 0.1366

[a] $R1 = \sum ||F_o| - |F_c|| / \sum |F_o|$. [b] $wR2 = [\sum w(|F_o^2| - |F_c^2|)^2 / \sum w|F_o^2|^2]^{1/2}$.

$w_1 = 1/[\sigma^2(F_o)^2 + 0.0594P^2 + 1.9874P]$, where $P = (F_o^2 + 2F_c^2)/3$. $w_2 = 1/[\sigma^2(F_o)^2 + 0.0733P^2 + 0.8069P]$, where $P = (F_o^2 + 2F_c^2)/3$. $w_3 = 1/[\sigma^2(F_o)^2 + 0.0863P^2 + 4.7182P]$, where $P = (F_o^2 + 2F_c^2)/3$.

Table 2. Crystallographic data for **4-6**.

Complexes	**4**	**5**	**6**
Formula	$C_{24}H_{13}CuN_3O_6$	$C_{50}H_{33}N_7Ni_2O_{14}$	$C_{48}H_{34}N_6NiO_{15}$
Fw	502.91	1073.25	993.52
Temperature(K)	293(2)	298(2)	293(2)
Wavelength(Å)	1.54178	0.71076	0.71073
Crystal system	Monoclinic	Monoclinic	Monoclinic
Space group	$P2_1/n$	$P2_1/c$	$P2_1/c$
a(Å)	13.276(3)	20.79(6)	11.7921(6)
b(Å)	13.867(3)	14.59(4)	16.3564(7)
c(Å)	16.406(3)	17.61(4)	23.2228(12)
α(deg)	90	90	90
β(deg)	111.90(3)	114.66(3)	100.938(2)
γ(deg)	90	90	90
V(Å^3)	2802.4(12)	4854(23)	4397.8(4)
Z	4	4	4
D_c(g·cm^{-3})	1.192	1.469	1.501
F(000)	1020	2200	2048
θ range for data collection(deg)	3.676~71.998	2.904~25.249	3.065~24.804
Reflections collected /unique	61376/5515	70946/8761	86061/7519
Data/restraints/	5515/0/308	8761/30/680	7519/13/664
Goodness-of-fit on F^2	0.825	1.030	1.083
Absorption coefficient	1.424	0.851	0.523
Tmin/Tmax	0.5306, 0.7536	0.6413, 0.7456	0.6787, 0.7451
Final R1[a], wR2[b]	0.0394, 0.1229	0.0612, 0.1367	0.0464, 0.0975

[a] $R1 = \sum ||F_o| - |F_c|| / \sum |F_o|$. [b] $wR2 = [\sum w(|F_o^2| - |F_c^2|)^2 / \sum w|F_o^2|^2]^{1/2}$.

$w_4 = 1/[\sigma^2(F_o)^2 + 0.0978P^2 + 3.4950P]$, where $P = (F_o^2 + 2F_c^2)/3$. $w_5 = 1/[\sigma^2(F_o)^2 + 0.0797P^2 + 0.8482P]$, where $P = (F_o^2 + 2F_c^2)/3$. $w_6 = 1/[\sigma^2(F_o)^2 + 0.0366P^2 + 5.1497P]$, where $P = (F_o^2 + 2F_c^2)/3$.

Table 3. Antimicrobial screening results of the H_3tpt ligands, **1**-**6** and metal salts.

Complexes and metal salts	Inhibition zone diameter (mm)			
	Bacillus subtilis	Staphylococcus aureus	Salmonella enteritidis	Escherichia coli
1	12.3	6.00	6.00	6.00
2	10	6.00	6.00	6.00
3	15.2	6.00	6.00	6.00
4	9.8	6.00	6.00	6.00
5	15	6.00	6.00	6.00
6	8	6.00	6.00	6.00
H_3tpt	6.00	6.00	6.00	6.00
$CuSO_4 \cdot 5H_2O$	6.00	6.00	6.00	6.00
$CuCl_2 \cdot 6H_2O$	6.00	6.00	6.00	6.00
$CuBr_2$	6.00	6.00	6.00	6.00
$NiCl_2 \cdot 6H_2O$	6.00	6.00	6.00	6.00
Control: DMSO	6.00	6.00	6.00	6.00

Table 4. Minimum inhibition concentration (MIC) values for **1**-**6** and some standard drugs.

Polymers and standard	MIC of Bacillus subtilis(μg/mL)
1	4
2	8
3	2
4	16
5	1
6	64
Kanamycin*	-
Streptomycin*	10
Gatifloxacin*	4.0
Norfloxacin*	2.5
Ciprofloxacin*	1.1
Sparfloxacin*	2.0

* Standard drug.

- Dashes indicated zero inhibition, all microorganisms were resistant to DMSO.

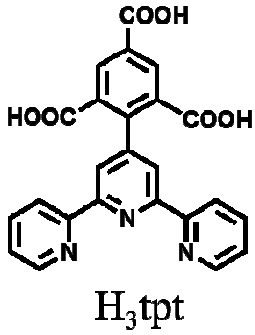

H_3tpt

Scheme 1. Structure of the H_3tpt ligand.

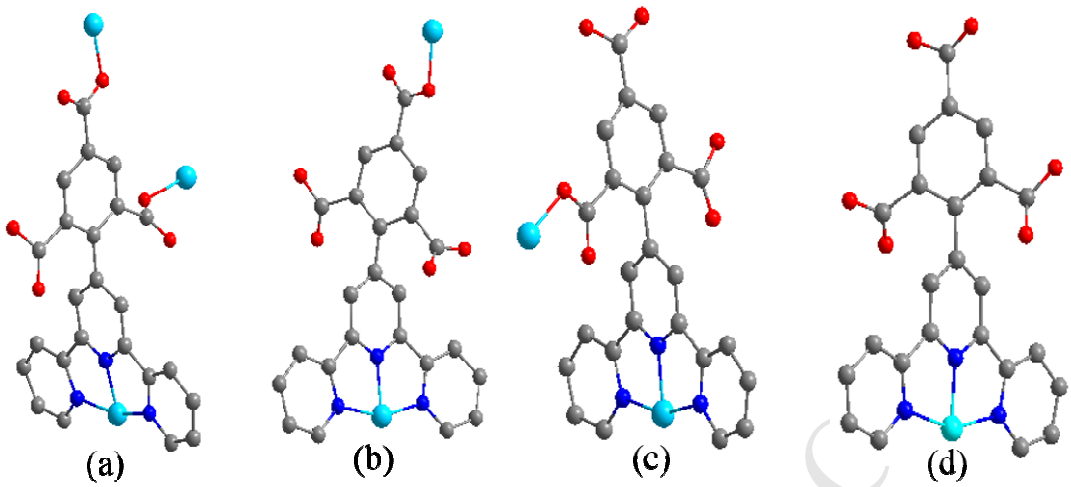

Scheme 2. (a) Coordination modes found in **1** and **5**. (b) Coordination modes found in **2**. (c) Coordination modes found in **3**. (d) Coordination modes found in **6**.

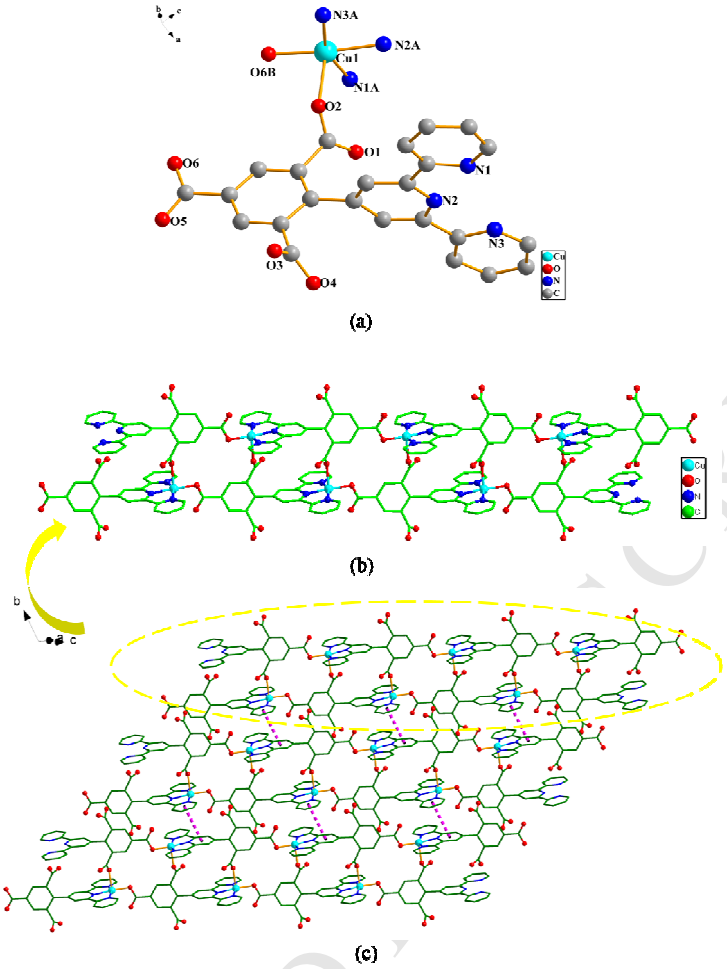

Figure 1. (a) The coordination environment of Cu(II) atom in **1** (A: 1-x, -y-1, -z+2; B: 2-x, -1-y, 3-z), all hydrogen atoms are omitted for clarity. (b) The 1-D double chains structure. (c) 2-D structure resulting from $\pi\cdots\pi$ stacking.

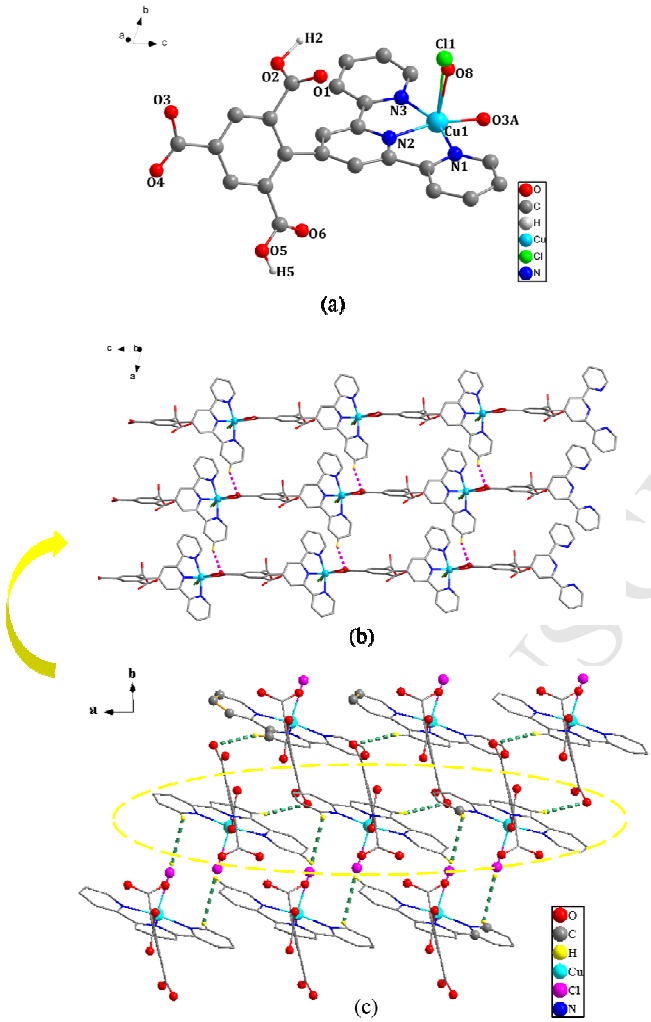

Figure 2. (a) The coordination environment of Cu(II) atom in **2** (A: x, y, z+1), part of the hydrogen atom is omitted for clarity. (b) The 2-D supramolecular structure. (c) 3-D supramolecular structure constructed by hydrogen-bonding interactions.

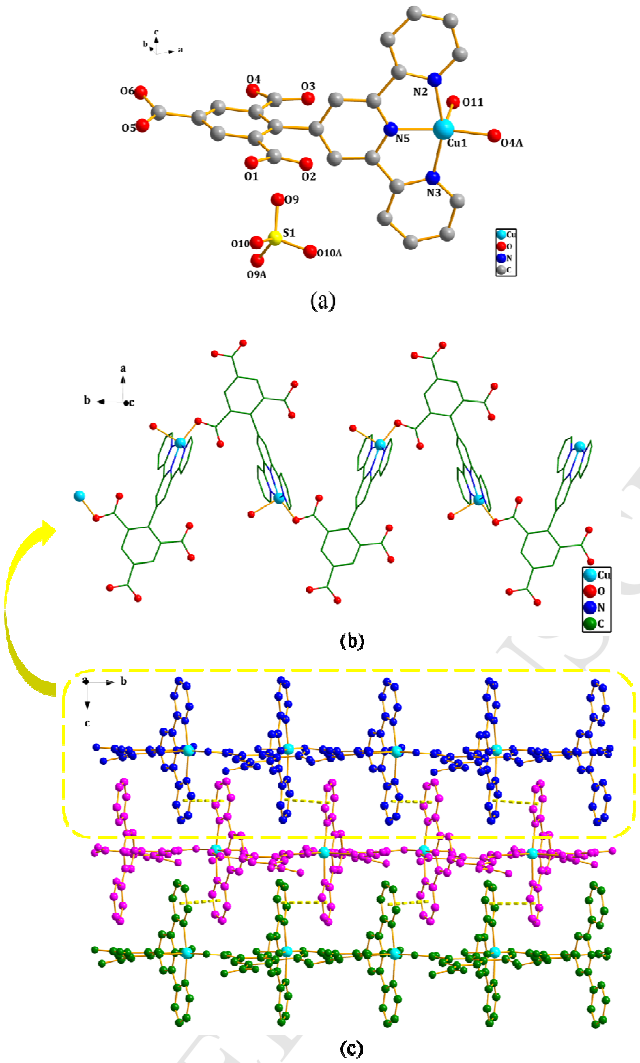

Figure 3. (a) The coordination environment of Cu(II) atom in **3** (A: -x+3/2, y-1/2, z), all hydrogen atoms are omitted for clarity. (b) The 1-D zigzag chains structure. (c) 2-D structure resulting from π··π stacking.

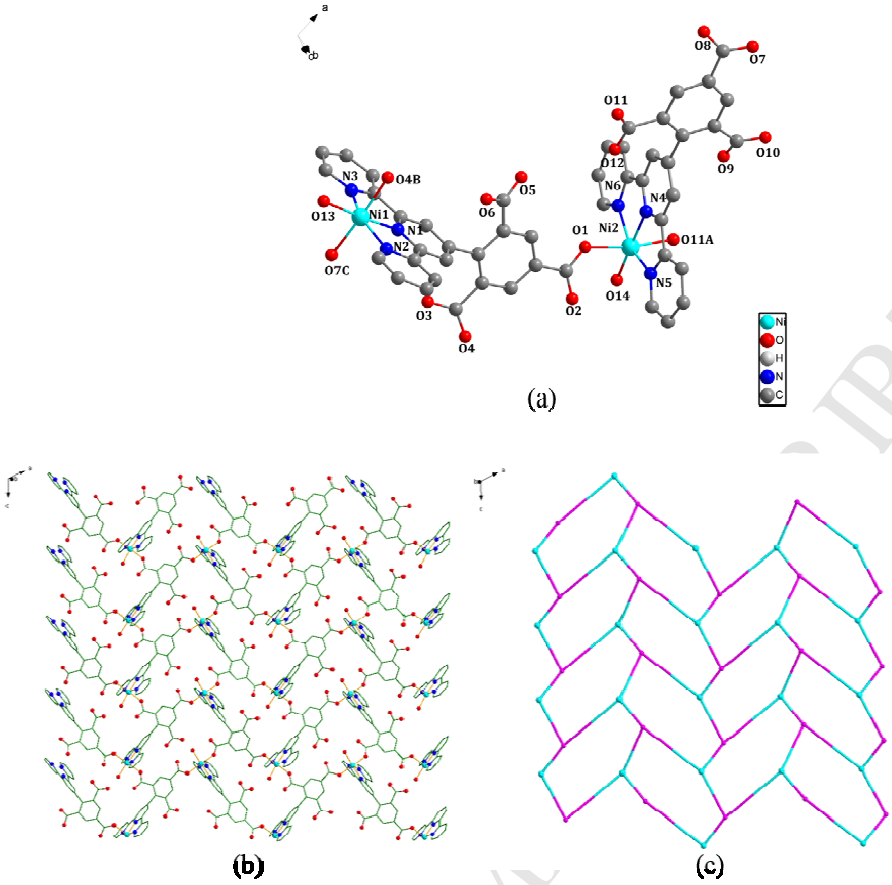

Figure 4. (a) The coordination environment of Ni(II) atom in **5** (A: x, -y+1/2, z+1/2; B: -1+x, -y+1/2, z-1/2), all hydrogen atoms are omitted for clarity. (b) The 2-D planar network. (c) Views of topology of **5** [The blue balls represent Ni(II) atoms, the pink balls represent the $Htpt^{2-}$ ligands, respectively].

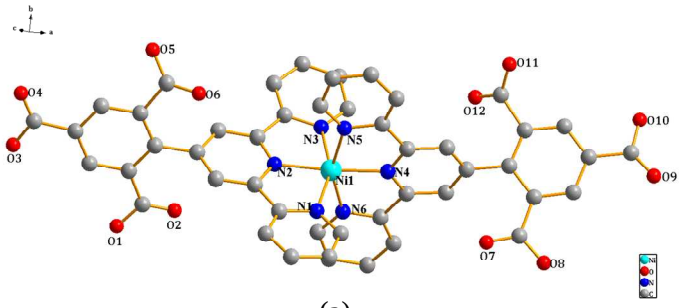

(a)

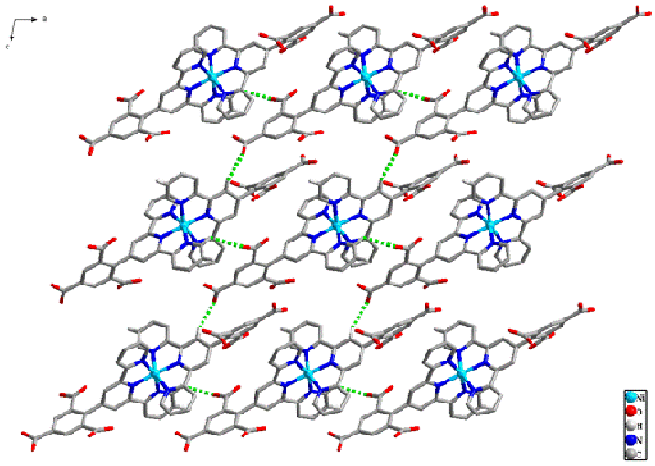

(b)

Figure 5. (a) The coordination environment of Ni(II) atom in **6**, all hydrogen atoms are omitted for clarity. (b) 2-D structure resulting from C-H···O hydrogen-bonding interactions.

Highlights:

1. Six complexes have been synthesized and characterized.
2. **1**-**3** show 1D structures, **4**-**5** are 2D frameworks and **6** is a mononuclear structure.
3. The relationship between the structures and antibacterial activities was studied.